Published in final edited form as:
Cerebellum. 2008 ; 7(3): 451–466. doi:10.1007/s12311-008-0049-5.

Both Cell-Autonomous and Cell Non-Autonomous Functions of GAP-43 are Required for Normal Patterning of the Cerebellum In Vivo

Yiping Shen,
Department of Anatomy and Cellular Biology, Tufts University School of Medicine, 136 Harrison Avenue, Boston, MA 02111, USA

Rashmi Mishra,
National Brain Research Center, Manesar, Haryana 122-050, India

Shyamala Mani, and
National Brain Research Center, Manesar, Haryana 122-050, India

Karina F. Meiri
Department of Anatomy and Cellular Biology, Tufts University School of Medicine, 136 Harrison Avenue, Boston, MA 02111, USA

Karina F. Meiri: karina.meiri@tufts.edu

Abstract

Growth-associated protein 43 (GAP-43) is required for development of a functional cerebral cortex in vertebrates; however, its role in cerebellar development is not well understood. Recently, we showed that absence of GAP-43 caused defects in proliferation, differentiation, and polarization of cerebellar granule cells. In this paper, we show that absence of GAP-43 causes defects in cerebellar patterning that reflect both cell-autonomous and non-autonomous functions. Cell-autonomous effects of GAP-43 impact precursor proliferation and axon targeting: In its absence, (1) proliferation of granule cell precursors in response to sonic hedgehog and fibroblast growth factor is inhibited, (2) proliferation of neuroepithelial precursors is inhibited, and (3) targeting of climbing fibers to the central lobe is disrupted. Cell non-autonomous effects of GAP-43 impact differentiated Purkinje cells in which GAP-43 has been downregulated: In its absence, both maturation and mediolateral patterning of Purkinje cells are inhibited. Both cell-autonomous and non-autonomous functions of GAP-43 involve its phosphorylation by protein kinase C. GAP-43 is phosphorylated in granule cell precursors in response to sonic hedgehog in vitro, and phosphorylated GAP-43 is also found in proliferating neuroepithelium and climbing fibers. Phosphorylated GAP-43 is specifically enriched in the presynaptic terminals of parallel and climbing fibers that innervate Purkinje cell bodies and dendrites. The cell-autonomous and non-autonomous effects of GAP-43 converge on the central lobe. The multiple effects of GAP-43 on

Correspondence to: Karina F. Meiri, karina.meiri@tufts.edu.

Yiping Shen and Rashmi Mishra contributed equally to this work.

cerebellar development suggest that it is a critical downstream transducer of signaling mechanisms that integrate generation of cerebellar structure with functional parcellation at the central lobe.

Keywords

GAP-43; Knockout mouse; Cerebellar granule cell proliferation; Purkinje cell patterning; Sonic hedgehog; Climbing fibers

Introduction

The highly ordered internal circuitry of the cerebellum belies its complex roles in the control of motor and cognitive functions. Precisely segregated input from climbing fibers (CFs) interacts with Purkinje cell (PC) output in three-dimensional modules or microzones, each having specific connections with spinal cord, brainstem, and cerebral cortex [25, 26]. Within the cerebellum, these microzones generate trans- and parlobular compartments [22, 31]. The molecular mechanisms that generate these functional compartments are not well understood, particularly with respect to how the extent of granule cell (GC) proliferation, largely controlled by sonic hedgehog (Shh, reviewed by [55]), is coupled to functional parcellation to determine input and output matching. In large part, this is due to the lack of markers that define the full extent of functional circuits (reviewed in [17, 20, 22, 62). Most markers of structural compartments within the cerebellum label only Purkinje cells and few of those persist throughout development [46]. Only one, the IQ-motif calmodulin-binding protein neurogranin, has been described for the period when CF inputs are synapsing onto PCs [32]. However, it labels only PC cell bodies and dendrites and its function in the organization of cerebellar compartments is unclear.

The growth-associated protein-43 (GAP-43) is also a member of the IQ-motif, calmodulin-binding protein family [16]. GAP-43 plays a major role in the developmental organization of the central nervous system (CNS) in vivo: Mice that do not express GAP-43 show extensive motor and sensory impairment [42]. They fail to form topographical maps in somatosensory, visual, and auditory cortices [37], and interhemispheric telencephalic connections are absent [53]. All stages of CNS development are vulnerable: neuronal proliferation in the subventricular zone (SVZ) is inhibited, axonal pathfinding is aberrant, and learning is impaired [37, 38, 48]. This modulation is dependent on protein kinase C (PKC) phosphorylation: In GAP-43 (+/−) commissural axons, 100% of which fail to cross the midline effectively, the defects directly correlate with the extent that GAP-43 in the affected axons is phosphorylated. In the cerebellum, we previously showed that GCs require GAP-43 to respond to Ig superfamily cell adhesion molecule (IgCAM) and fibroblast growth factor (FGF) signals that regulate neurogenesis and neurite outgrowth [41]. We have also recently shown that GAP-43 plays a critical role in the proliferation, differentiation, and polarization of granule cell precursors (GCPs) [43]. These effects echo its role in the cell division of cerebral cortical precursors [56]. In this paper, we extend those studies to show that both cell-autonomous and non-autonomous functions of GAP-43 are required for cerebellar development. Thus, neurogenesis of PCs is inhibited and the GC response to FGF and Shh is aberrant. Moreover, afferent cerebellar inputs are also disrupted in an IgCAM-associated

manner. The defects converge at the central lobe, which is particularly vulnerable to absence of GAP-43. The results suggest that GAP-43 is a critical downstream transducer of signaling mechanisms that integrate generation of cerebellar structure with functional parcellation at the central lobe.

Materials and Methods

Genotyping of GAP-43 Knockout Mice

GAP-43-deficient mice were generated from targeted CJ7 ES cells in isogenic 129S3/imJ mice (genetic designation+Mgf-SlJ, JAX stock number 002448) and backcrossed for eight to 12 generations with C57BL/6N. Homozygote (−/−) mice were identified by polymerase chain reaction genotyping as described previously [37]. In all cases, mice were anesthetized with xylazine/ketamine administered i.p. (12.5– 25 mg/kg body weight). All animal experiments were performed in strict accordance with NIH guidelines and approved by the Institutional Animal Care and Use Committee.

Histology and Immunocytochemistry

For histological and immunohistochemical analysis, a minimum of three animals from each genotype were analyzed. Fresh brains were briefly soaked in India ink to reveal surface morphology. Otherwise, brains were fixed in 4% paraformaldehyde (PFA) before histological or immunochemical staining with either pan-GAP-43 mab 7B10 or phospho-specific GAP-43 mab 2G12 [40]; calbindin (Sigma, St Louis, MO, USA), patched (Ptc-1), sonic hedgehog (Shh), smoothened (Smo; all from Abcam, Cambridge, MA, USA); βIII tubulin (Covance, Berkeley, CA, USA); phosphohistone H3 (Sigma). For heat shock protein 25 immunohistochemistry (HSP-25, Research Diagnostics Inc, Flanders, NJ, USA), the fix also contained 0.01% glutaraldehyde. Postnatal animals were fixed by perfusion, whereas embryonic and neonatal animals were fixed by immersion. Fixed brains were either paraffin-embedded or cryostat sectioned sagittally at 10 μm except for HSP-25 immunohistochemistry, which used 50-μm vibratome sections. Parasagittal sections were demonstrated to be at the midline (vermis) by absence of cortical neurons and olfactory bulb. Cerebellar structures were revealed by Nissl or hematoxylin and eosin (H&E) staining. For immunostaining, sections were permeabilized with 0.02% digitonin (Sigma). In some cases (e.g., Ptc-1, Shh, and Smo labeling), antigen retrieval was carried out by steaming the sections for 20 min in 0.1 M citrate buffer, pH 6.9 in a commercially available steamer (Black and Decker, Miramar, FL, USA). Immunoreactivity was either detected with isotype-specific fluorochrome-conjugated secondary antibodies or was amplified using biotin-conjugated secondary antibody together with fluorochrome-conjugated tertiary antibody. In each case, antibodies were obtained from Jackson (West Grove, PA, USA). Confocal images were collected using a Leica TCS SP2 confocal microscope using the same settings (Ar laser line, 488-nm laser excitation wavelength, 0.5-μm-thick optical sections, 28 z-series sections for each sample). All immunohistochemical and immunocytochemical experiments using similar antibodies were performed in parallel on comparable GAP-43 (+/+) and (−/−) material and photographed under the same settings to allow direct comparison.

Post Hoc Manipulation of Digital Images

Digital images were collected in Photoshop. All images were processed with the 'unsharp mask' filter. Images were corrected for exposure and color balance. Any digital manipulations to enhance brightness or contrast were performed on each GAP-43 (+/+) and (−/−) image in parallel.

In Vivo BrDU Labeling

To label proliferating cells, mice received a single intraperitoneal injection of bromodeoxyuridine (BrDU, Sigma) at a dose of 10 μg/g body weight. After 2 h, animals were anesthetized, as described above, brains were dissected, immersion fixed in Omni-II fixative (FR Chemicals, Mount Vernon, NY, USA), paraffin-embedded, and serially sectioned sagittally at 7 μm. Midsagittal sections from GAP-43 (+/+) and (−/−) mice were treated with 6 N HCl to denature DNA before incubating with anti-BrDU antibody (BD Biosciences, San Jose, CA, USA). Immunoreactivity was visualized with fluorescein-isothiocyanate-conjugated secondary antibody, and cells were counterstained with 4′,6-diamidino-2-phenylindole dihydrochloride (DAPI) to label nuclei. The labeling index in the cerebellar primordium was ascertained from the ratio of Brdu-labeled cells and DAPI-labeled nuclei using Axiovision software version 3.1 (Zeiss). Cells in a total of three medial and three lateral sections from each animal were counted using three animals per genotype.

Quantification of Cerebellar Morphology, Granule Cell Density, Proliferating Cells, and Staining Intensity

Folia size and fissure depth were measured on digital images collected from H&E- and Nissl-stained midsagittal sections at the vermis using IP Lab software (Scanalytics). Fissure depth was measured as described previously [60]. Intensity of staining with Shh signaling pathway components was measured from high power confocal images by segmentation analysis of defined regions of interest using the IPLAB program (Scanalytics). Ten independent areas from each section were quantitated. A total of six sections from each genotype were used.

Cerebellar Cultures

Dissociated cultures of P5 cerebella enriched in GCPs were prepared as before [15, 43] and plated at a density of 2×10^4 cells/cm^2 onto poly-D-lysine-coated Labtek chambers (Nalge/Nunc, Rochester, NY, USA). After 9 to 12 h at 37°C in 0.5% CO_2, the medium was replaced with Dulbecco's modified Eagle's medium (DMEM)-F-12 for 1 h to downregulate serum-responsive signaling mechanisms and then changed to DMEM-F-12 containing N2 supplement and 25 mM KCl. For cell proliferation studies, cells were cultured for 24 h with 10 μM BrDU added during the initial 12 h. In some cases, 3 μg/ml Shh, 25 ng/ml basic FGF (R&D Systems), or Shh + 1 μg/ml of the Shh inhibitor cyclopamine (EMD Chemicals, San Diego, CA, USA) were also added. Cells processed for protein analysis by sodium dodecyl sulfate– polyacrylamide gel electrophoresis and Western blotting were lysed in solutions containing 20 mM sodium fluoride and 2 mM sodium orthovanadate [52]. Immunoreactivity to 2G12 was detected with HRP-conjugated secondary antibody and ECL reagent (Amersham Biosciences). Total GAP-43 signal was obtained by stripping and reprobing

with the pan-GAP-43 antibody 7B10. Exposure of the film (Hyper-film, Amersham) was kept within the linear range and band intensity quantified using NIH Image software (National Institutes of Health, Bethesda, MD, USA).

Results

Effects on Development of Folia and Lobules

We examined cerebellar structure postnatally at P0, when the primary lobes are first beginning to be established, and at P21 when foliation is complete. Hereafter, the nomenclature used is that employed by Altman and Bayer [2] in their classic textbook on cerebellar development. At P0, when the primary (cardinal) fissures (f1-4) had begun to form, parasagittal sections showed that the external circumference at the vermis was already reduced by 33% (measured between the asterisks in Fig. 1a,b). Invagination of the primary fissure (fpr), the secondary fissure (fsec), and the precentral (fprc) were reduced. Defects occurred in 100% of the backcross GAP-43 (−/−) mice and in none of their GAP-43 (+/+) littermates. Hence, the GAP-43 (−/−) cerebellum is defective even before expansion of GCs has begun.

At P21, parasagittal sections showed that the external circumference at the vermis was still reduced by 25% in all GAP-43 (−/−) animals (measured between the asterisks, Fig. 1c,d). Most primary and secondary fissures were shorter (Table 1). The anterior part of the central lobe (CeL, comprising folia VIa, VIb, and VII) was reduced most (57%). Within the CeL, three distinct structural phenotypes were evident involving the fiber bundle that normally penetrates lobule VI (middle arrow in Fig. 1d), the fps, and the fiber bundle that normally penetrates lobule VII (arrow in Fig. 1c). In each case, they were significantly attenuated or absent (also illustrated in Fig. 7). Next, the anterior part of the anterior lobe (anterobasal, folia I and II) was reduced by 43% because the precentral fissure (fprc) was significantly shorter. Finally, the inferior lobe (IL, folia IXa-c) was reduced by 34% because the uvular sulcus (s.uv) was significantly shorter (lower arrow in Fig. 1d). The phenotype was 100% penetrant in the GAP-43 (−/−) 129S3/imJ-C57BL/6N backcross animals. Only the posterior part of the anterior lobe (anterodorsal) approximated wild-type size. This was because an intraculminate fissure (ficul) separating folia IV and V (upper arrow in Fig. 1d) now appeared in 100% of GAP-43 (−/−) cerebella. The ficul was also present in >50% of (+/+) backcross mice. Hence defects in the GAP-43 (−/−) cerebellum persist during formation of the secondary fissures.

Examining the surface structure of the cerebellum after 7 months confirmed that defects in the central lobe also persisted during maturity. At the vermis, a separation between folia VI and VII, corresponding to the fps, could not be distinguished. In addition to its normal association with the simplex lobe and crus 1, lobule VI was also now associated with the hemispheric lobes crus II (CII) and the paramedian lobe (P, arrows in Fig. 1e,f). Hereafter, we focus on the GAP-43-dependent cellular phenotypes occurring in lobules VIa, VIb, and VII of the CeL at the vermis.

Effects on Sonic Hedgehog and FGF-Mediated Regulation of Granule Cell Proliferation and Differentiation

Formation of the secondary fissures occurs as a result of GC proliferation between P3-P7. We have recently shown that the defects when GAP-43 is absent are due in large part to the reduced expansion of GCPs. In the absence of GAP-43, proliferation of GCPs is inhibited, and they differentiate prematurely both in vitro and in vivo. Immature GC neurons also fail to polarize appropriately because of mispositioning of the centrosome at the final mitosis, so that migration is also abnormal [43].

Proliferation and differentiation of GCPs are driven by Shh and basic fibroblast growth factor (bFGF) [10]. To investigate whether GAP-43 (−/−) GCPs respond to Shh and bFGF normally, we treated cerebellar granule cells in culture with each mitogen. In cultures of wild-type GCs taken at P5, the time when proliferation is maximal in vivo, Shh increased the labeling index of GCPs (L.I., the percentage of cells incorporating bromodeoxyuridine compared with total) by 282% compared with untreated control cultures (100%, Fig. 2a), but only by 159% when GAP-43 was absent. Nonetheless, most of the cells that incorporated BrDU subsequently progressed to express βIII tubulin, so that some expansion of the neuronal population occurred as it does in vivo (Fig. 2a). bFGF also increased the L.I. of GC cultures by 233%, but only by 143% when GAP-43 was absent. We have previously shown that GAP-43 is directly involved in the bFGF signaling pathway: GAP-43 is the major neuronal substrate of PKC [7], and PKC-phosphorylated GAP-43 can be detected with a specific antibody, 2G12, that recognizes the single PKC phosphorylation site on ser41 [40] (Fig. 2b). In GC cultures, bFGF stimulates phosphorylation of GAP-43 [41]. Likewise, Shh also stimulated phosphorylation of GAP-43 in GC cultures: 2G12 immunoreactivity increased, while GAP-43 levels were unaffected, suggesting that GAP-43 is also located directly downstream in the Shh signaling pathway. This was confirmed with the Shh antagonist cyclopamine. Shh-mediated increases in GAP-43 phosphorylation were completely inhibited by concurrent treatment of the cultures with 5 nM cyclopamine. To determine how Shh signaling in vivo is impacted by absence of GAP-43, we examined distribution of the inhibitory Shh receptor patched-1 (Ptc-1), the excitatory Shh receptor smoothened (Smo), and Shh itself in lobules VI and VII of the CeL, the area most affected by absence of GAP-43. In GAP-43 (+/+) cerebella, Ptc-1, Smo, and Shh were all expressed in the external granule cell layer (EGL) as well as by PCs that were identified by calbindin immunoreactivity (Fig. 2c, inset). In the EGL, absence of GAP-43 resulted in upregulation of Ptc-1 and downregulation of Smo in the inner EGL (asterisks Fig. 2d,h). In PCs, Ptc-1 expression was uniform (Fig. 2c), but both Shh (Fig. 2e) and Smo (Fig. 2g) were patchily distributed around the fppd. In the absence of GAP-43, expression of the Shh signaling components at the fppd was quantitatively altered: Ptc-1 expression in PCs was significantly decreased by 2.8-fold from 182±33 (SD) to 65±9 arbitrary fluorescence units ($p< 0.03$, Mann–Whitney test, $n=6$ (Fig. 2d). Conversely, the patches without high levels of Shh and Smo immunoreactivity expanded (Fig. 2g,h). Hence, absence of GAP-43 exerts effects on PCs in the affected area of the CeL, even though at this stage, PCs no longer express GAP-43 ([9], discussed in full below).

Cell-Autonomous Effects on Prenatal Development of the Cerebellum

Together, the previous results demonstrate that GAP-43 exerts both cell-autonomous and non-autonomous effects on cerebellar development. To parse out how this might transpire, we first examined the cerebellar anlage, focusing on the fate of cells that normally express GAP-43, and in which, therefore, effects of its absence are expected to be cell-autonomous. The PKC phosphorylated form of GAP-43 (pGAP-43) is enriched in mitosing cells in both the subventricular zone of the cerebral cortex and the EGL of the cerebellum ([56], [43]). PGAP-43 was likewise detected in mitosing cells in the neuroepithelium at E12.5 (Fig. 3a, insert) the time when PCs are born [2, 24, 39]. In the absence of GAP-43, the L.I. in the neuroepithelium was significantly decreased relative to wild type (Fig. 3b). Shortly after their birth, PCs begin to migrate perpendicular to the cerebellar cortex [2]. We previously showed that migration of GCs in vivo was abnormal in the absence of GAP-43 [43]. Likewise, migration of GAP-43 (−/−) TuJ-1-labeled neurons from the neuroepithelium was inhibited, and the neurons appeared misaligned (compare ‘a’ arrows Fig. 3c,d). Prenatal effects of GAP-43 were not limited to PCs migrating from the neuroepithelium: Neurons of the deep cerebellar nuclei are born in the rhombic lip between E13 and E16.5 and migrate parallel to the cerebellar cortex in the nuclear transitory zone [36]. At E13.5, GAP-43 (−/−) neurons migrating from the rhombic lip also appeared decreased (compare ‘b’ arrows Fig. 3c,d). Increased Nissl labeling adjacent to the neuroepithelium was indicative of increased cell density, offering further evidence that cell migration was inhibited (Fig. 3f). Also at E13.5, the neurofilament antigen recognized by the 2H3 antibody labeled fibers that will form the hook bundle (arrow, Fig. 3e). This too was reduced in the absence of GAP-43 (bottom arrow, Fig. 3f).

By E15.5, migrating PCs in the cerebellar anlage expressed both calbindin [8] (Fig. 4a) and the immunoglobulin superfamily antigen DM-GRASP that is recognized by the BEN antibody [12] (Fig. 4b). In contrast, GAP-43 was not expressed by differentiating calbindin or BEN-labeled PCs that were migrating from the neuroepithelium (insert Fig. 4c), although there was strong labeling in the fibrous zone (arrow Fig. 4c [2]) and in the region where the future CeL will develop (asterisk Fig. 4c), the first evidence of an enrichment of GAP-43 in this specific region (see below).

Cell Non-Autonomous Effects on Postnatal Purkinje Cell Development

Consistent with the inhibition of proliferation in the embryonic neuroepithelium, numbers of mature PCs were reduced. As a consequence, the average linear density of GAP-43 (−/−) PCs at P21 was not significantly different from (+/+) littermates, (63±7 cells/mm vs. 58±4 cells/ mm, n=6), even though the cerebellum itself was smaller. Likewise, consistent with the delayed migration in the embryonic neuroepithelium, migration of PCs was abnormal: In wild-type cerebella at P0, migrating PCs were beginning to coalesce subjacent to the ML (asterisks Fig. 5a,c), except in the CeL from which they are normally excluded [46] (arrows, Fig. 5a,c). In the absence of GAP-43, this coalescence of PCs was delayed, and they appeared clumped (asterisks, Fig. 5d). PCs also invaded the CeL (arrows, Fig. 5b,d). Hence, early effects of GAP-43 on PC differentiation had persistent postnatal consequences.

Conversely, postnatal PC development that could not directly be ascribed to prior impairment of proliferation and migration was also abnormal in GAP-43 (−/−) cerebella. In wild-type cerebella at P8, PCs surrounding the primary and secondary fissures had formed a monolayer and elaborated dendritic arbors (Fig. 5e). In the absence of GAP-43, monolayer formation was delayed and the dendritic arbors of the PCs were stunted compared with wild type and appeared misaligned (arrows, Fig. 5e,f). By P21, PCs flanking the primary fissures, such as the fpr, had formed a monolayer even in the absence of GAP-43 (not shown); however, those surrounding the affected secondary fissures, such as the fppd, remained aggregated especially at the fissure flanks (arrows, Fig. 5h).

Cell-Autonomous Effects on Innervation of the Cerebellum

Innervation of the CeL was particularly vulnerable to absence of GAP-43. As demonstrated above, the fiber bundles that normally penetrate lobe VI and lobe VII were severely attenuated. We therefore examined the effect of GAP-43 on development of innervation of the CeL. At E17.5, the neurofilament antigen 2H3 detected fibers within the cerebellar peduncle (Cp, Fig. 6a) as well as fibers within nascent cerebellar compartments (arrows, Fig. 6a) [2]. At this time, GAP-43-expressing fibers were specifically targeted to the nascent CeL (arrow, Fig. 6b). In its absence, the cerebellar anlage itself was smaller, and there were fewer 2H3-labeled fibers (asterisk, Fig. 6c). At P0, the βIII tubulin antibody TuJ-1 labeled the fiber tracts underlying the primary lobes identified by Altman and Bayer [2] as anterobasal, (ABT); anterodorsal, (ADT), and central, (CeT). TuJ-1 also labeled the molecular layer (arrow, Fig. 6d) and the fastigial nucleus (FN). GAP-43 was expressed by all the tracts in the anterior and central cerebellum (ABT, ADT, and CeT), as well as by the posterior tract (POT) that did not label with TuJ-1. However, it was only highly expressed by ML neurons in the CeL (asterisk, Fig. 6e). Moreover, GAP-43 was highly phosphorylated in both the CeT fibers that terminated in the CeL (Fig. 6f) and in neurons in the ML overlying the CeL (asterisk, Fig. 6f). In the absence of GAP-43, TuJ-1 labeling showed that the CeT fibers targeted to the CeL were dramatically reduced (arrow, Fig. 6g) and that the ML neurons in the CeL were specifically decreased (asterisk, Fig. 6g). Hence, the fiber tracts that are particularly susceptible to the absence of GAP-43 are those with axons in which phosphorylated GAP-43 is enriched. These fibers co-localized in the CeL with ML neurons in which GAP-43 is also highly phosphorylated.

We used two further markers to verify that the interaction between CeT fibers and ML neurons was disrupted when GAP-43 is absent. CeT fibers and ML neurons in the anterior cerebellum also expressed 2H3 (Fig. 6h), and a subset of the CeT fibers that terminated in the CeL co-expressed NCAM (arrow, Fig. 6h). NCAM-expressing ML neurons were interposed between unlabeled EGL (vertical arrow, Fig. 6h) and unlabeled migrating PCs (horizontal arrow, Fig. 6h). In fact, the region at which CeT fibers and ML neurons colocalize in the CeL was that from which migrating PCs are normally excluded at P0 (see Fig. 6). In the absence of GAP-43, NCAM/2H3-labeled CeT fibers did not penetrate the CeL in either midline (not shown) or lateral sections (illustrated, arrow Fig. 6i). Moreover, NCAM-expressing ML neurons could not be detected in the ML of the CeL (asterisk, Fig. 6h). Hence, in the absence of GAP-43, CeT and ML neurons fail to co-localize in the CeL, and ectopic PCs populate that area (see Fig. 6).

To examine the nature of the CeT and ML neurons containing highly phosphorylated GAP-43, we first examined climbing fibers that synapse on PC cell bodies and proximal dendrites [2]. At P21, the BEN antibody detected climbing fiber input that terminates in the AL and CeL (Fig. 7a–d) [8]. In the absence of GAP-43, BEN labeling of fibers in the AL and CeL was significantly reduced overall (Fig. 7c,d). Moreover, at high power, few BEN-labeled axons were detected in lobes VI and VII of the CeL (compare arrows in Fig. 7b,d), and they appeared misaligned (compare inserts in Fig. 7b,d).

Consequences on Purkinje Cell Output

We next examined the location of phosphorylated GAP-43 in the ML. Output from the cerebellum is modulated by synapses between PCs and both climbing fibers, which innervate cell bodies and proximal dendrites, and parallel fibers of GCs, which innervate distal dendrites. At P21, phosphorylated GAP-43 was enriched in presynaptic terminals that synapsed on PC cell bodies and both proximal and distal dendrites (Fig. 7e–h). This phosphorylation was non-uniform and defined parlobular patches leaving other areas devoid of phosphorylated GAP-43 (asterisks, Fig. 7g). Parlobular mediolateral stripes in folia VI–VIII in the CeL can also be detected with heat shock protein 25 (HSP-25 [3]; Fig. 6i,j) that labels PC dendrites. In the absence of GAP-43, the parlobular stripe pattern of PCs at the vermis was disrupted (asterisks, Fig. 6j). In this instance, because the fps was missing at the vermis, lobules VI and VII appeared fused. Hence, absence of GAP-43 causes disruption of mediolateral parlobular compartments in the CeL of the cerebellum.

Discussion

Our results here show that GAP-43, a protein associated with regulation of neurogenesis, axon guidance, and long-term potentiation in cerebral cortex, is also required for patterning of the cerebellum, particularly at the vermis. GAP-43 had both cell-autonomous and cell non-autonomous roles in cerebellar patterning: The former involved regulation of granule cell and neuroepithelial precursor proliferation and targeting of cerebellar afferents. The latter involved regulation of postnatal Purkinje cell development. Both roles were correlated with phosphorylation of GAP-43 by PKC. All homozygote GAP-43 (−/−) cerebella were affected. Together with our previous results showing that absence of GAP-43 disrupts neurogenesis in cerebral cortex, prevents formation of the telencephalic commissures, and disrupts thalamocortical projections causing failure to form topographic maps, they pinpoint GAP-43 as a major contributor to CNS organization in vertebrates.

With respect to the cell-autonomous roles of GAP-43 on GCs, we have previously shown that GAP-43 is required for the proliferation and differentiation of GCPs [41, 43]. The balance between proliferation and differentiation of GCPs is regulated by the intersection between FGF and Shh signaling, with Shh stimulating GC proliferation and FGF stimulating proliferation or differentiation depending on temporal context [11, 14, 63]. Previously, we showed that FGF-mediated differentiation of GCs (measured by increased numbers of cells extending neurites) is dependent on GAP-43 and directly correlated with increased phosphorylation of GAP-43 by PKC [41] consistent with GAP-43 location downstream in the FGF signaling pathway [6]. Here, we show that both FGF- and Shh-mediated

proliferation (measured by increased L.I. following BrDU incorporation) are also GAP-43-dependent. Moreover, like FGF, Shh directly increased GAP-43 phosphorylation by PKC, consistent with data from mouse ES cells that the ability of Shh to activate its downstream targets to stimulate proliferation depends on activation of PKC [23]. Hence, the localization of GAP-43 downstream of both the FGF and Shh signaling pathway suggests that it is a component of an intracellular node involving PKC at which FGF and Shh signaling intersect [14]. Between P5-P7, when the effects of GAP-43 on Shh proliferation were evident in vitro, GCs in vivo express the inhibitory Shh receptor Ptc-1 [59] as well as GAP-43 [9, 43]. Ptc-1 function is dependent on membrane-dependent regulation of the actin cytoskeleton [18] as well as extracellular factors [19, 50]. GAP-43 modulates F-actin interaction with membranes [33], and F-actin is reduced in GAP-43 (−/−) GCs as it is in cerebral cortical neurons [43]. Our results therefore support the notion that cell-autonomous roles of GAP-43 in Shh signaling reflect its actin-regulatory ability at the cell membrane.

Consistent with our immunohistochemical data, PCs are the major source of the Shh in the postnatal cerebellar cortex (reviewed in [61]). However, in contrast with GCs, postnatal PC neurons do not express GAP-43 (see also [9]). Hence, the downregulation of Shh, Ptc-1, and Smo in GAP-43 (−/−) PCs cannot reflect a cell-autonomous effect of GAP-43 on an autocrine function of Shh analogous to that occurring in the embryo where autocrine activity of Shh regulates PC development [11]. This is the first time that GAP-43 has been associated with Shh signaling in any system.

Cell-autonomous roles of GAP-43 in PC development occur only during early development of the cerebellar anlage where the inhibited neurogenesis in the GAP-43 (−/−) neuroepithelium resembles that seen in the SVZ of the GAP-43 (−/−) cerebral cortex [38]. In both those cases, it is the phosphorylated form of GAP-43 that is enriched in the mitosing cells [56] as it is in mitosing GCs [43]. In GCs, absence of GAP-43 results in profound effects on cell cycle regulation that are associated with defects in the mitotic spindle and centrosome positioning. Whether this is a common mechanism that also underlies defects in the SVZ and neuroepithelium remains to be established. The reduced numbers of mature PCs strongly supports the notion that absence of GAP-43 affects proliferation of PCs in the neuroepithelium; however, lack of a marker for the earliest PC precursors precludes, conclusively proving this supposition. Neurogranin, the earliest endogenous PC marker in mice is unequivocally present only once PCs have differentiated at E15 [31]. Hence, we cannot rule out that some of the reduced proliferation reflects effects on inferior olivary precursors that arise from the precerebellar primary neuroepithelium [58]. Notwithstanding, GAP-43 is not clearly not expressed by PCs between E15.5 and E17.5, as was shown previously by in situ hybridization (http://www.gensat.org). Thus, the impaired migration of GAP-43 (−/−) PCs at this time may either reflect a transition to a cell non-autonomous role or the consequences of a cell-autonomous effect that occurred during a previous cell division. In this regard, inappropriate process extension and aberrant migration of GAP-43 (−/−) GCs in vivo is due to mispositioning of the centrosome at the prior final mitosis [43]. Whether a similar mechanism underlies the aberrant PC migration in the cerebellar anlage remains to be established. We detected no increase in apoptosis of mature PCs that would account for the reduction in numbers (not shown).

Cell non-autonomous effects of GAP-43 on PC development become unambiguous postnatally after its expression has been downregulated for many days. They most likely involve interactions with GCs in which GAP-43 is still expressed. PCs and GCs develop symbiotically: Full arborization of PC dendrites depends on the presynaptic activity of the presynaptic parallel fiber synapses in which GAP-43 is enriched [13] and in which GAP-43 is patchily phosphorylated by PKC. Similar phosphorylation of GAP-43 by PKC is also crucial in the hippocampus for modulation of long-term potentiation [49], strongly suggesting that GAP-43 in parallel fiber terminals also plays a PKC-dependent modulatory role that is crucial for PC development.

It is not yet clear how the morphological phenotype of mature GAP-43 (−/−) PCs arises. The stunted and misaligned PC dendrites resemble those from BDNF- or NT3-deficient mice [51], suggesting an indirect effect of defective BDNF signaling. A relationship between GAP-43 and BDNF in GCs has been established: GAP-43 is upregulated in GCs following BDNF treatment in vitro [5, 51] and GAP-43 (−/−) GCs do not respond to BDNF in a neurite outgrowth assay (not shown). How this may impact development of PC remains to be investigated.

GAP-43 exerts clear cell-autonomous effects on cerebellar afferents that innervate the CeL, particularly those fibers that express immunoglobulin superfamily cell adhesion molecules (IgSF-CAMs). Perinatally, the afferents targeted to the CeL that were specifically disrupted expressed the IgSFCAM NCAM. In the mature cerebellum, the afferents targeted to lobules VI and VII that were specifically disrupted expressed the IgSFCAM DMGRASP [12]. The well-documented role of GAP-43 in IgSFCAM signaling is dependent on its phosphorylation by PKC [28, 34, 41]. Hence, the disrupted circuitry when GAP-43 is absent suggests that IgSFCAM signaling via GAP-43 may confer identity to a specific compartment in the CeL, such as has been described previously [46]. Whether GAP-43 signaling in the different cell types (CFs and parallel fibers) and their impact on a specific subset of PCs defines a functional microzone remains to be established [47].

In that regard, our results showing a role for GAP-43 in cerebellar patterning are reminiscent of some of GAP-43 functions in cerebral cortex: There, GAP-43 is required for somatotopically organized input from the ventrobasal nucleus of the thalamus that defines somatosensory and whisker barrel maps [37]. In the cerebellum, GAP-43 is required for the topographically organized CF input from the medial accessory olive (MAO) to lobule VIa [57]. Both the ventrobasal nucleus VB and the MAO are innervated in a crudely somatotopic fashion (e.g., [44]), and both lack any obvious structural abnormalities in the absence of GAP-43 ([37], not shown). The GAP-43 (−/−) phenotype resembles the *wv/wv* mutation in which the regional specificity that derives from the climbing fiber afferents innervating the CeL is disrupted without olivary topography being grossly affected [4]. In that case, however, the distribution of NCAM labeled fibers was unaffected, suggesting that the underlying mechanism is different [27]. With respect to function, the heavy phosphorylation of GAP-43 in the presynaptic terminals of CF and parallel fibers innervating PCs strongly suggests that it is involved in modulation of cerebellar output. In the cerebral cortex, PKC phosphorylation of GAP-43 in presynaptic terminals enhances visual learning in specific circuits [64]. Not all the roles of GAP-43 in the cerebellum have parallels in cerebral cortex

and vice versa: For instance, non-cell-autonomous roles for GAP-43, as reflected in the vulnerability of the PCs in lobule VI, have yet not been described in cerebral cortex. Conversely, heterozygote GAP-43 (+/−) mice also display strong phenotypes only in the cerebral cortex, but not in the cerebellum. Presumably, there is increased molecular redundancy in the cerebellum, reflecting its more ancient evolutionary origin.

Two major questions are still outstanding: First, what are the downstream molecular targets of GAP-43? In both proliferating neuronal precursors and axons, PKC phosphorylation of GAP-43 determines how membrane-signaling modules interact with the actin cytoskeleton [21, 28, 30, 45, 43]. Moreover, like neurogranin and PEP 19, both of which are involved in cerebellar patterning (Hockberger et al. 2004; [32]), GAP-43 is an IQ motif calmodulin binding protein. How those two functions, and the other IQ-motif family members, interact to define compartments in the CeL of the vermis remains to be established. Second, what may the functional consequences of the defects in cerebellar structure be? The sexually mature GAP-43 (−/−) mouse displays behavioral abnormalities that reflect disrupted control of motor functions [29, 42]. Our preliminary results suggest that some of these functions are sex linked with a disproportionate effect on males (Nguyen and Meiri, unpublished observations). Although we found no sex-linked differences in cerebellar structure, GAP-43 expression is known to be regulated by estrogen and sexually dimorphic in the cerebral cortex [35, 54]. Whether disruptions in the connections between the cerebral and cerebellar cortices underlie the functional phenotype remains to be established.

Acknowledgments

We thank Dr William Brunken for initially alerting us to the cerebellar phenotype, Dr Richard Hawkes for helpful discussions and Lilly Nguyen for expert technical assistance. This work was supported by NS33118 (KFM) and an NIH R03TW0605 Fogarty International Award (KFM and SM).

Abbreviations

ABT	anterobasal tract
ADT	anterodorsal tract
AL	anterior lobe
BrDU	bromodeoxyuridine
CeL	central lobe
CeT	central tract
CF	climbing fiber
Cp	cerebellar peduncle
EGL	external granule cell layer
FGF	fibroblast growth factor
FN	fastigial nucleus
GAP-43	growth-associated protein 43

GC	granule cell
GCP	granule cell precursor
IgSFCAM	immunoglobulin superfamily cell adhesion molecule
LI	labeling index
ML	molecular layer
NCAM	neural cell adhesion molecule
PC	Purkinje cell
PCP	Purkinje cell precursor
PKC	protein kinase C
PL	posterior lobe
Ptc-1	patched-1
POT	posterior tract
Shh	sonic hedgehog
Smo	smoothened
SVZ	subventricular zone

References

1. Altman J, Bayer SA. Development of the precerebellar nuclei in the rat: 11. The intramural olivary migratory stream and the neurogenetic organization of the inferior olive. J Comp Neurol. 1987; 257:490–512. [PubMed: 3693595]
2. Altman, J.; Bayer, SA. CRC. New York: 1996. Development of the cerebellar system.
3. Armstrong CL, Krueger-Naug AM, Currie RW, Hawkes R. Constitutive expression of the 25-kDa heat shock protein Hsp25 reveals novel parasagittal bands of Purkinje cells in the adult mouse cerebellar cortex. J Comp Neurol. 2000; 416:383–397. [PubMed: 10602096]
4. Blatt GJ, Eisenman LM. The olivocerebellar projection in normal (+/+), heterozygous weaver (*wv*/+), and homozygous weaver (*wv/wv*) mutant mice: comparison of terminal pattern and topographic organization. Exp Brain Res. 1993; 95:187–201. [PubMed: 7693502]
5. Borghesani PR, Peyrin JM, Klein R, Rubin J, Carter AR, Schwartz PM, Luster A, Corfas G, Segal RA. BDNF stimulates migration of cerebellar granule cells. Development. 2002; 129:1435–1442. [PubMed: 11880352]
6. Cavallaro U, Niedermeyer J, Fuxa M, Christofori G. N-CAM modulates tumour-cell adhesion to matrix by inducing FGF-receptor signalling. Nat Cell Biol. 2001; 3:650–657. [PubMed: 11433297]
7. Chan SY, Murakami K, Routtenberg A. Phosphoprotein F1: purification and characterization of a brain kinase C substrate related to plasticity. J Neurosci. 1986; 6:3618–3627. [PubMed: 3794793]
8. Chedotal A, Pourquie O, Ezan F, San Clemente H, Sotelo C. BEN as a presumptive target recognition molecule during the development of the olivocerebellar system. J Neurosci. 1996; 16:3296–3310. [PubMed: 8627367]
9. Console-Bram LM, Fitzpatrick-McElligott SG, McElligott JG. Distribution of GAP-43 mRNA in the immature and adult cerebellum: a role for GAP-43 in cerebellar development and neuroplasticity. Brain Res Dev Brain Res. 1996; 95:97–106.
10. Corrales JD, Blaess S, Mahoney EM, Joyner AL. The level of sonic hedgehog signaling regulates the complexity of cerebellar foliation. Development. 2006; 133:1811–1821. [PubMed: 16571625]

11. Dahmane N, Ruiz i Altaba A. Sonic hedgehog regulates the growth and patterning of the cerebellum. Development. 1999; 126:3089–3100. [PubMed: 10375501]
12. DeBernardo AP, Chang S. Heterophilic interactions of DM-GRASP: GRASP-NgCAM interactions involved in neurite extension. J Cell Biol. 1996; 133:657–666. [PubMed: 8636239]
13. Drake-Baumann R. Rapid modulation of inhibitory synaptic currents in cerebellar Purkinje cells by BDNF. Synapse. 2005; 57:183–190. [PubMed: 15986361]
14. Fogarty MP, Emmenegger BA, Grasfeder LL, Oliver TG, Wechsler-Reya RJ. Fibroblast growth factor blocks sonic hedgehog signaling in neuronal precursors and tumor cells. Proc Natl Acad Sci U S A. 2007; 104:2973–2978. [PubMed: 17299056]
15. Gao WO, Heintz N, Hatten ME. Cerebellar granule cell neurogenesis is regulated by cell-cell interactions in vitro. Neuron. 1991; 6:705–715. [PubMed: 2025426]
16. Gerendasy D. Homeostatic tuning of Ca^{2+} signal transduction by members of the calpacitin protein family. J Neurosci Res. 1999; 58:107–119. [PubMed: 10491576]
17. Goldowitz D, Hamre K. The cells and molecules that make a cerebellum. Trends Neurosci. 1998; 21:375–382. [PubMed: 9735945]
18. Gonzalez-Quevedo R, Shoffer M, Horng L, Oro AE. Receptor tyrosine phosphatase-dependent cytoskeletal remodeling by the hedgehog-responsive gene MIM/BEG4. J Cell Biol. 2005; 168:453–463. [PubMed: 15684034]
19. Guerrero I, Chiang C. A conserved mechanism of hedgehog gradient formation by lipid modifications. Trends Cell Biol. 2007; 17:1–5. [PubMed: 17126548]
20. Hatten ME, Heintz N. Mechanisms of neural patterning and specification in the developing cerebellum. Annu Rev Neurosci. 1995; 18:385–408. [PubMed: 7605067]
21. He Q, Dent EW, Meiri KF. Modulation of actin filament behavior by GAP-43 (neuromodulin) is dependent on the phosphorylation status of serine 41, the protein kinase C site. J Neurosci. 1997; 17:3515–3524. [PubMed: 9133376]
22. Herrup K, Kuemerle B. The compartmentalization of the cerebellum. Annu Rev Neurosci. 1997; 20:61–90. [PubMed: 9056708]
23. Heo JS, Lee MY, Han HJ. Sonic Hedgehog stimulates mouse embryonic stem cell proliferation by cooperation of Ca^{2+}/ protein kinase C and EGF receptor as well as Gli1 activation. Stem Cells. 2007; 12:3069–3080. [PubMed: 17901397]
24. Inouye M, Murakami U. Temporal and spatial patterns of Purkinje cell formation in the mouse cerebellum. J Comp Neurol. 1980; 194:499–503. [PubMed: 7451678]
25. Ito M. The molecular organization of cerebellar long-term depression. Nat Rev Neurosci. 2002; 3:896–902. [PubMed: 12415297]
26. Ito M. Cerebellar circuitry as a neuronal machine. Prog Neurobiol. 2006; 78:272–303. [PubMed: 16759785]
27. Jorgensen OS. Neural cell adhesion molecule and D3 protein in the cerebellum of weaver mutant mice. Int J Dev Neurosci. 1994; 12:213–225. [PubMed: 7942094]
28. Korshunova I, Novitskaya V, Kiryushko D, Pedersen N, Kolkova K, Kropotova E, Mosevitsky M, Rayko M, Morrow JS, Ginzburg I, Berezin V, Bock E. GAP-43 regulates NCAM-180-mediated neurite outgrowth. J Neurochem. 2007; 100:1599–1612. [PubMed: 17212696]
29. Koyner J, Demarest K, McCaughran J Jr, Cipp L, Hitzemann R. Identification and time dependence of quantitative trait loci for basal locomotor activity in the BXD recombinant inbred series and a B6D2 F2 intercross. Behav Genet. 2000; 3:159–170. [PubMed: 11105390]
30. Larsson C. Protein kinase C and the regulation of the actin cytoskeleton. Cell Signal. 2006; 18:276–284. [PubMed: 16109477]
31. Larouche M, Hawkes R. From clusters to stripes: the developmental origins of adult cerebellar compartmentation. Cerebellum. 2006; 5:77–88. [PubMed: 16818382]
32. Larouche M, Che PM, Hawkes R. Neurogranin expression identifies a novel array of Purkinje cell parasagittal stripes during mouse cerebellar development. J Comp Neurol. 2006; 494:215–227. [PubMed: 16320235]

33. Laux T, Fukami K, Thelen M, Golub T, Frey D, Caroni P. GAP43, MARCKS, and CAP23 modulate PI(4,5)P(2) at plasmalemmal rafts, and regulate cell cortex actin dynamics through a common mechanism. J Cell Biol. 2000; 149:1455–1472. [PubMed: 10871285]
34. Leshchyns'ka I, Sytnyk V, Morrow JS, Schachner M. Neural cell adhesion molecule (NCAM) association with PKCbeta2 via betaI spectrin is implicated in NCAM-mediated neurite outgrowth. J Cell Biol. 2003; 161:625–639. [PubMed: 12743109]
35. Lustig RH, Hua P, Wilson MC, Federoff HJ. Ontogeny, sex dimorphism, and neonatal sex hormone determination of synapse-associated messenger RNAs in rat brain. Brain Res Mol Brain Res. 1993; 20:101–110. [PubMed: 8255171]
36. Machold R, Fishell G. Math1 is expressed in temporally discrete pools of cerebellar rhombic-lip neural progenitors. Neuron. 2005; 48:17–24. [PubMed: 16202705]
37. Maier DL, Mani S, Donovan SL, Soppet D, Tessarollo L, McCasland JS, Meiri KF. Disrupted cortical map and absence of cortical barrels in growth-associated protein (GAP)-43 knockout mice. Proc Natl Acad Sci U S A. 1999; 96:9397–9402. [PubMed: 10430954]
38. Mani S, Shen Y, Schaefer J, Meiri KF. Failure to express GAP-43 during neurogenesis affects cell cycle regulation and differentiation of neural precursors and stimulates apoptosis of neurons. Mol Cell Neurosci. 2001; 17:54–66. [PubMed: 11161469]
39. Maricich SM, Herrup K. Pax-2 expression defines a subset of GABAergic interneurons and their precursors in the developing murine cerebellum. J Neurobiol. 1999; 41:281–294. [PubMed: 10512984]
40. Meiri KF, Bickerstaff LE, Schwob JE. Monoclonal antibodies show that kinase C phosphorylation of GAP-43 during axonogenesis is both spatially and temporally restricted in vivo. J Cell Biol. 1991; 112:991–1005. [PubMed: 1705561]
41. Meiri KF, Saffell JL, Walsh FS, Doherty P. Neurite outgrowth stimulated by neural cell adhesion molecules requires growth-associated protein-43 (GAP-43) function and is associated with GAP-43 phosphorylation in growth cones. J Neurosci. 1998; 18:10429–10437. [PubMed: 9852580]
42. Metz GA, Schwab ME. Behavioral characterization in a comprehensive mouse test battery reveals motor and sensory impairments in growth-associated protein-43 null mutant mice. Neuroscience. 2004; 129:563–574. [PubMed: 15541878]
43. Mishra R, Gupta SK, Meiri KF, Fong M, Thostrup P, Juncker D, Mani S. GAP-43 is key to mitotic spindle control and centrosome-based polarization in neurons. Cell Cycle. 2008; 7:348–357. [PubMed: 18235238]
44. Molinari HH, Schultze KE, Strominger NL. Gracile, cuneate, and spinal trigeminal projections to inferior olive in rat and monkey. J Comp Neurol. 1996; 375:467–480. [PubMed: 8915843]
45. Niethammer P, Delling M, Sytnyk V, Dityatev A, Fukami K, Schachner M. Cosignaling of NCAM via lipid rafts and the FGF receptor is required for neuritogenesis. J Cell Biol. 2002; 157:521–532. [PubMed: 11980923]
46. Ozol K, Hayden JM, Oberdick J, Hawkes R. Transverse zones in the vermis of the mouse cerebellum. J Comp Neurol. 1999; 412:95–111. [PubMed: 10440712]
47. Pijpers A, Apps R, Pardoe J, Voogd J, Ruigrok TJ. Precise spatial relationships between mossy fibers and climbing fibers in rat cerebellar cortical zones. J Neurosci. 2006; 26:12067–12080. [PubMed: 17108180]
48. Rekart JL, Meiri K, Routtenberg A. Hippocampal-dependent memory is impaired in heterozygous GAP-43 knockout mice. Hippocampus. 2005; 15:1–7. [PubMed: 15390153]
49. Routtenberg A, Cantallops I, Zaffuto S, Serrano P, Namgung U. Enhanced learning after genetic overexpression of a brain growth protein. Proc Natl Acad Sci U S A. 2000; 97:7657–7662. [PubMed: 10861025]
50. Rubin JB, Choi Y, Segal RA. Cerebellar proteoglycans regulate sonic hedgehog responses during development. Development. 2002; 129:2223–2232. [PubMed: 11959830]
51. Schwartz PM, Borghesani PR, Levy RL, Pomeroy SL, Segal RA. Abnormal cerebellar development and foliation in BDNF −/− mice reveals a role for neurotrophins in CNS patterning. Neuron. 1997; 19:269–281. [PubMed: 9292718]

52. Sharma SK, Carew TJ. Inclusion of phosphatase inhibitors during Western blotting enhances signal detection with phospho-specific antibodies. Anal Biochem. 2002; 307:187–189. [PubMed: 12137799]
53. Shen Y, Mani S, Donovan SL, Schwob JE, Meiri KF. GAP-43 is required for commissural axon guidance in the developing vertebrate nervous system. J Neurosci. 2002; 22:239–247. [PubMed: 11756507]
54. Shughrue PJ, Dorsa DM. The ontogeny of GAP-43 (neuromodulin) mRNA in postnatal rat brain: evidence for a sex dimorphism. J Comp Neurol. 1994; 340:174–184. [PubMed: 8201017]
55. Sotelo C. Cellular and genetic regulation of the development of the cerebellar system. Prog Neurobiol. 2004; 72:295–339. [PubMed: 15157725]
56. Stricker SH, Meiri K, Götz M. P-GAP-43 is enriched in horizontal cell divisions throughout rat cortical development. Cereb Cortex. 2006; 16(Suppl 1):121–131.
57. Sugihara I, Shinoda Y. Molecular, topographic, and functional organization of the cerebellar cortex: a study with combined aldolase C and olivocerebellar labeling. J Neurosci. 2004; 24:8771–8785. [PubMed: 15470143]
58. Taber-Pierce E. Histogenesis of the deep cerebellar nuclei in the mouse: an autoradiographic study. Brain Res. 1975; 95:503–518. [PubMed: 1156884]
59. Traiffort E, Charytoniuk D, Watroba L, Faure H, Sales N, Ruat M. Discrete localizations of hedgehog signalling components in the developing and adult rat nervous system. Eur J Neurosci. 1999; 11:3199–3214. [PubMed: 10510184]
60. Wahlsten D, Andison M. Patterns of cerebellar foliation in recombinant inbred mice. Brain Res. 1991; 557:184–189. [PubMed: 1747752]
61. Wallace VA. Purkinje-cell-derived sonic hedgehog regulates granule neuron precursor cell proliferation in the developing mouse cerebellum. Curr Biol. 1999; 9:445–448. [PubMed: 10226030]
62. Wang VY, Rose MF, Zoghbi HY. Math1 expression redefines the rhombic lip derivatives and reveals novel lineages within the brainstem and cerebellum. Neuron. 2005; 48:31–43. [PubMed: 16202707]
63. Wechsler-Reya RJ, Scott MP. Control of neuronal precursor proliferation in the cerebellum by sonic hedgehog. Neuron. 1999; 22:103–114. [PubMed: 10027293]
64. Zhang GR, Wang X, Kong L, Lu XG, Lee B, Liu M, Sun M, Franklin C, Cook RG, Geller AI. Genetic enhancement of visual learning by activation of protein kinase C pathways in small groups of rat cortical neurons. J Neurosci. 2005; 25:8468–8481. [PubMed: 16162929]

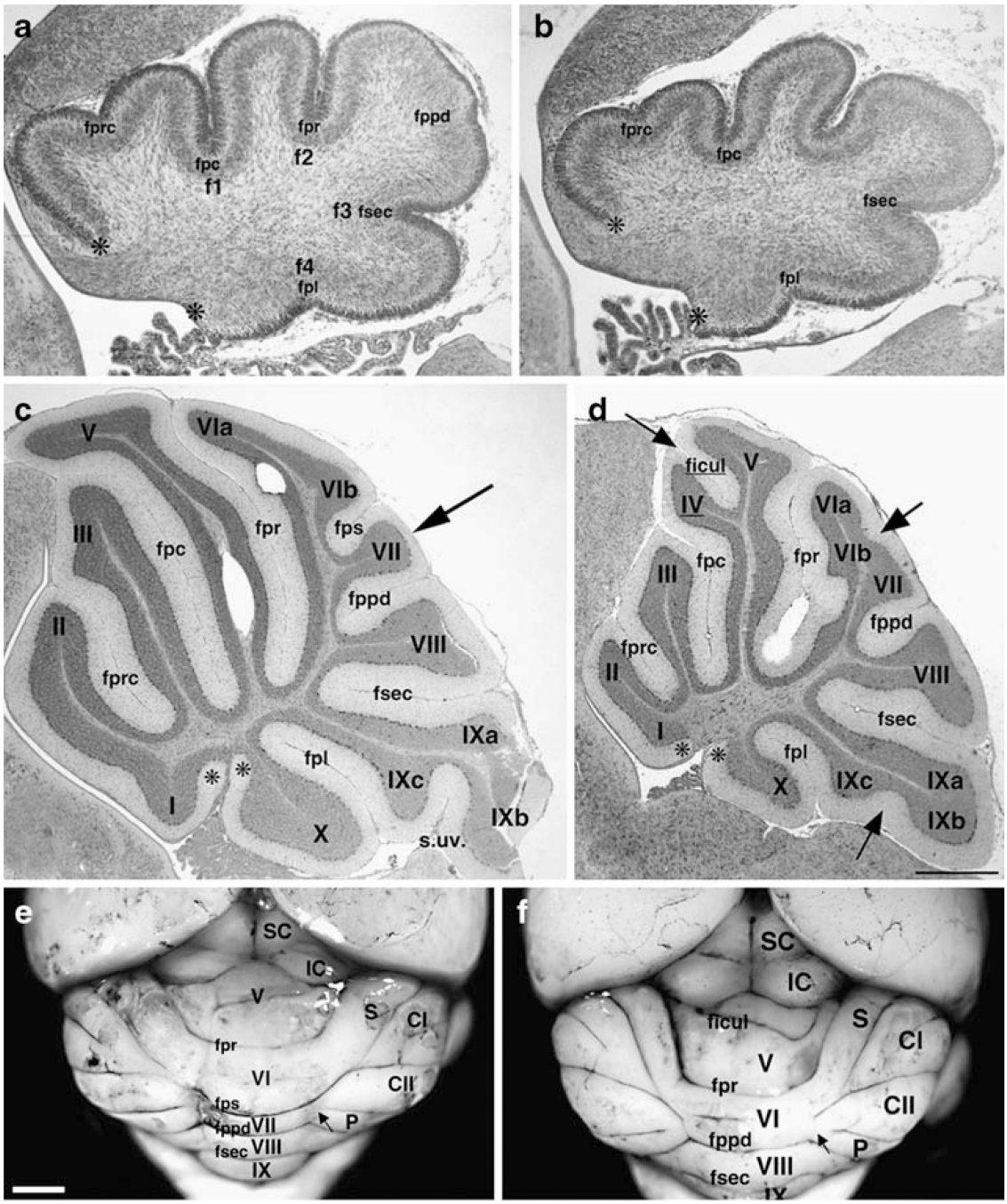

Fig. 1.

Structural abnormalities in the postnatal cerebellum. **a, b** Development of the primary lobes at P0: GAP-43 (+/+) (**a**) and GAP-43 (−/−) (**b**). **a** Primary fissures (*f1-4*) and the precentral fissure (*fprc*) in the anterior lobe (*AL*) are present. The prepyramidal fissure (*fppd*) in the central lobe (*CeL*) is beginning to invaginate. **b** The primary fissures are shorter and invagination of the fprc and fppd are delayed. *Asterisks* designate the boundaries of the external circumference measured. Scale bar=250 μm. **c, d** Midsagittal lobes at P21: GAP-43 (+/+) (**c**) and GAP-43 (−/−) (**d**). Anterior lobe (*AL*), I–V; central lobe (*CeL*), VI–VII;

posterior lobe (*PL*), VIII; nodular lobe (*NL*), IX–X. The primary fissure (*fpr*) separates the AL from the CeL. The secondary fissures of the AL are the precentral fissure (*fprc*) and the preculminate fissure (*fpc*). The prepyramidal fissure (*fppd*) separates the CeL from the PL. The secondary fissure of the CeL is the posterior superior fissure (*fps*). The secondary fissure (*fsec*) separates the PL from the NL. The secondary fissure of the NL is the posterolateral fissure (*fpl*). **c** *Arrow* indicates the fiber branch absent or attenuated in GAP-43 (−/−) mice. **d** *Arrows* indicate significantly altered fissures and sulci. Scale bar=100 μm. **e, f** Surface appearance of 7-month-old cerebella revealed with India ink: GAP-43 (+/+) (**e**) and GAP-43 (−/−) (**f**). Roman numerals *V–IX* indicate folia at the vermis. Lobes at the hemispheres are: *S* simplex, *CI* crus I, *CII* crus II, *P* paramedial, *F* paraflocculus. Visible fissures at the vermis: primary fissure (*fpr*); posterior superior fissure (*fps*); prepyramidal fissure (*fppd*); secondary fissure (*fsec*); intraculminate fissure (*ficul*). Superior colliculus (*SC*) and inferior colliculus (*IC*). *Arrows* indicate where the lateral lobes intersect with the vermis. Scale bar=1 mm (*n*=18 mice examined from each genotype)

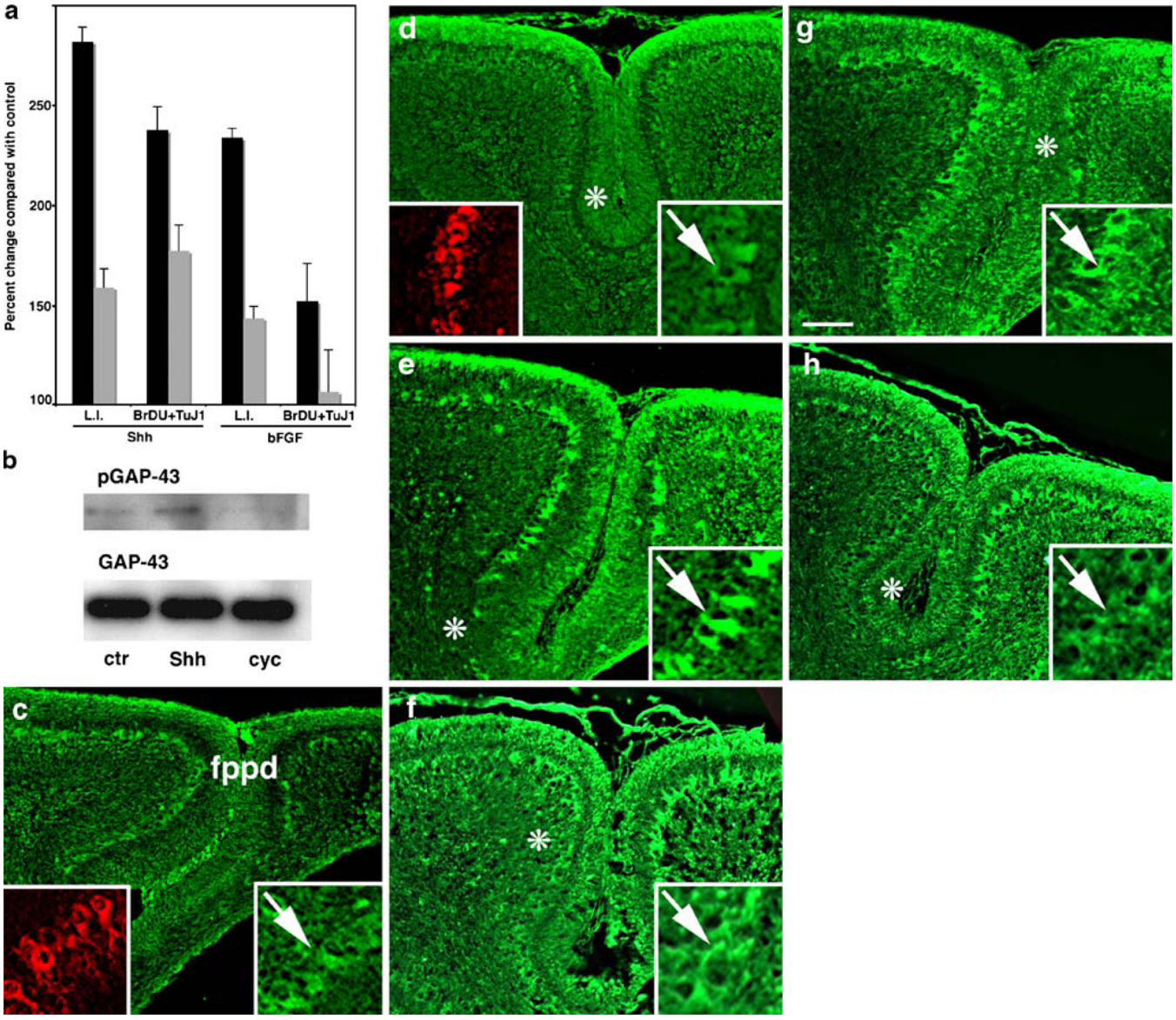

Fig. 2.

Regulation of Shh and FGF signaling in granule cells by GAP-43. **a** Percent change in the labeling index of GC cultures in vitro at P5 to Shh and FGF treatment compared with control cultures (no treatment) measured by BrDU incorporation. GAP-43 (+/+), *black bars*; GAP-43 (−/−), *white bars*. In the absence of GAP-43, the ability of both Shh and βFGF to stimulate BrDU incorporation was reduced, whereas the proportion of cells that had incorporated BrDU also labeled with the βIII tubulin antibody TuJ-1 was unaffected (n=6 mice from each genotype). For L.I. $p<0.01$ (−/−) Shh and FGF compared with (+/+) Mann–Whitney test. **b** Western blots from GAP-43 (+/+) GC cultures incubated ±3 μg/ml Shh or ±Shh + 5 nM cyclopamine. *Top* GAP-43 phosphorylation was detected with anti-phosphoGAP-43 antibody 2G12. *Bottom* Blots were stripped and reprobed with total GAP-43 antibody 7B10 to show equivalent loading. Stimulation of GAP-43 phosphorylation by Shh is inhibited by cyclopamine treatment. **c–f** Expression of Shh signaling molecules in

the CeL at P7. In each case, immunoreactivity around the fppd is illustrated. GAP-43 (+/+) (**c, e, g**) and GAP-43 (−/−) (**d, f, h**). **c, d** The inhibitory receptor Ptc-1 is expressed in the outer EGL (*asterisk* in **c**) and in PCs (*arrows* in high power insets [2.5×], *green*). Calbindin immunoreactivity confirms Ptc-1 localization in PCs (*arrows* in high power insets [2.5×], *red*). **d** In the absence of GAP-43, Ptc-1 is downregulated in PCs that retain calbindin expression (*arrow*). **e, f** Shh is expressed in the outer EGL and is patchily distributed in PCs (*asterisks* in **d**, *arrows* in high power insets [2.5×]). **f** In the absence of GAP-43, the patches in which Shh is expressed at low levels by PCs increase (*asterisk* in **f**). **g, h** The excitatory receptor Smo is also patchily expressed by PCs (*asterisk* in **g**, *arrows* in high power insets [2.5×]). **h** In the absence of GAP-43, the patches in which Smo is expressed at low levels by PCs increase (*asterisk* in **h**). Note the misalignment of PCs in **d, f**, and **h**. Scale bar (**c, d**)=500 μm; (**e–h**)= 400 μm

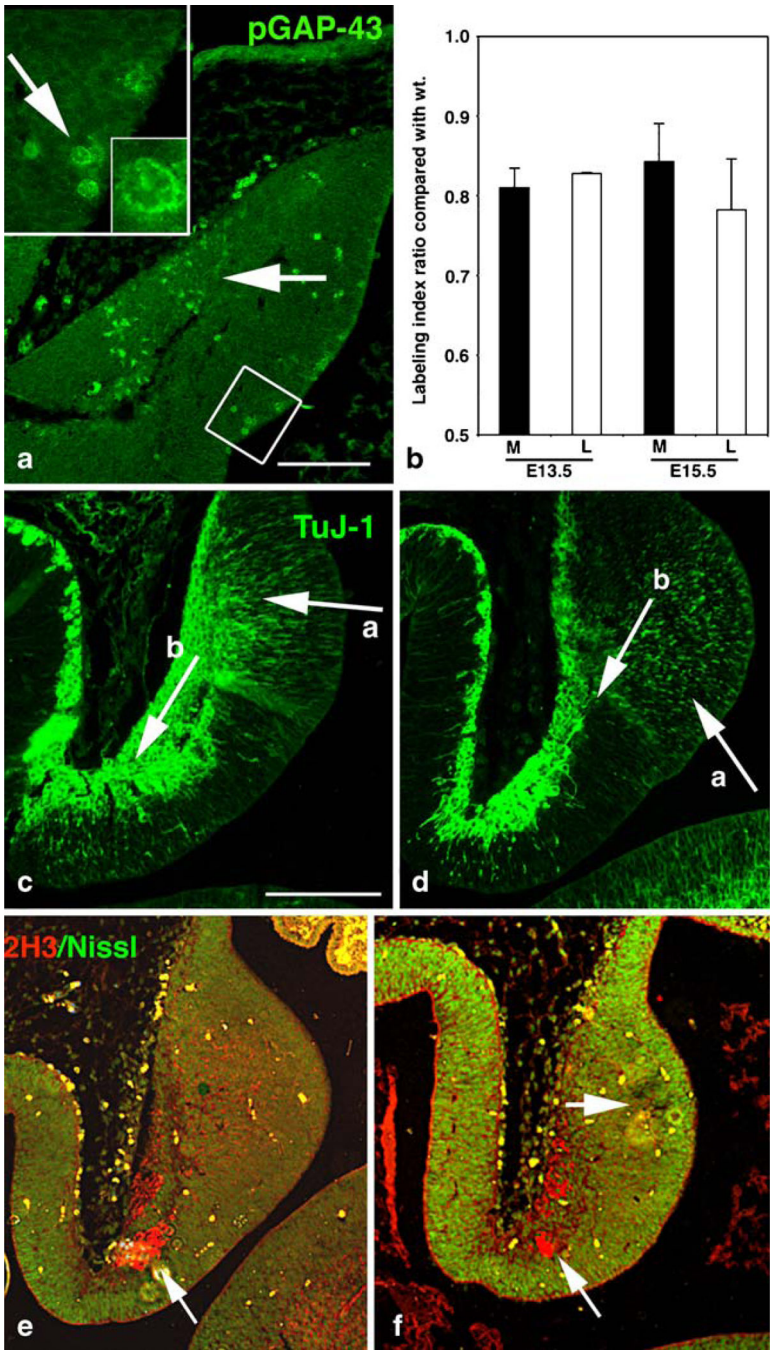

Fig. 3.

Defects in neuronal proliferation and migration in the cerebellar anlage. **a** Localization of pGAP-43 in the midsagittal cerebellar anlage at E12.5. Phospho-GAP-43 is enriched in cells in the neuroepithelium having mitotic figures (high power insets 2.5×, *arrow* 10×) and in migrating neurons (*arrow*). Scale bar=250 μm. **b** Change in the labeling index of GAP-43 (−/−) neuroepithelial cells from medial (*black*) and lateral (*white*) sections at E13.5 and E15.5, measured by BrDU incorporation and expressed as a ratio compared to GAP-43 (+/+). The L.I. was reduced in both areas compared with wild type. **c–f** Midsagittal sections

from the cerebellar anlage at E13.5. GAP-43 (+/+) (**c, e**), GAP-43 (−/−) (**d, f**). **c, d** TuJ-1 labels neurons migrating from the neuroepithelium (*arrow*, **a**) and from the rhombic lip (*arrow*, **b**). **d** In the absence of GAP-43, TuJ-1 label is decreased and migration of both neuroepithelial neurons (*arrow* in **a**) and rhombic lip neurons (*arrow* in **b**) appears delayed. **e, f** 2H3 labels neurons of the hook bundle (uncinate tract, bottom arrows) and fluorescent Nissl stain (*green*) detects cell density. **f** In the absence of GAP-43, fewer neurons are labeled with 2H3 (*bottom arrow*). However, fluorescent Nissl label is increased (*upper arrow*) consistent with inhibited differentiation and/or migration from the neuroepithelium. Scale bar=300 μm

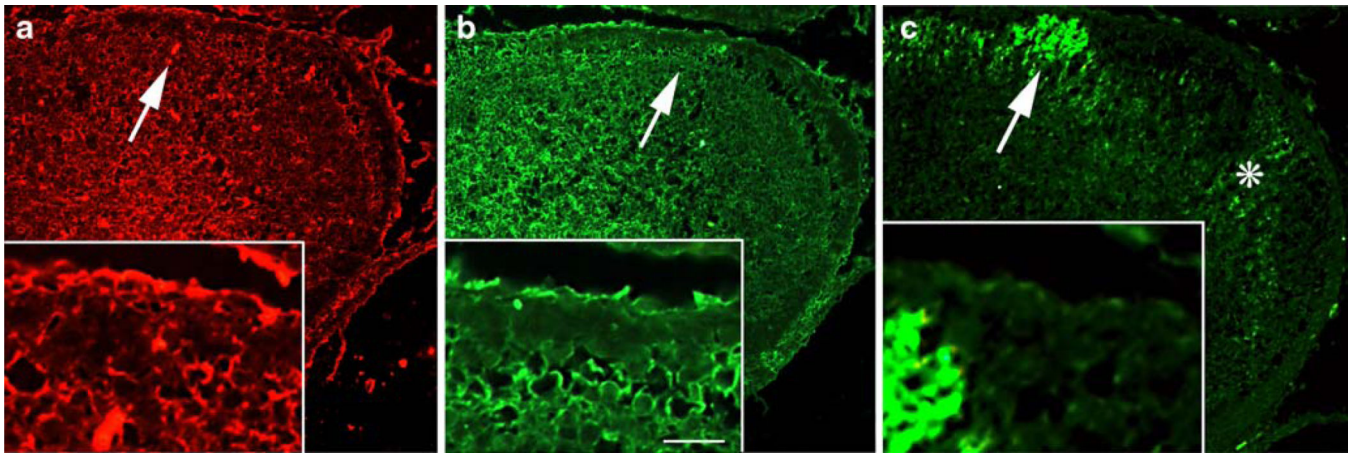

Fig. 4.

Initial differentiation of neurons in the cerebellar anlage. **a–c** Expression of neuronal markers in the GAP-43 (+/+) E15.5 midsagittal cerebellar anlage. **a** Calbindin labels differentiating PCs migrating toward cerebellar cortex. **b** BEN also labels differentiating neurons in the same region. **c** GAP-43 immunoreactivity does not overlap with either calbindin or BEN but is concentrated in the fibrous zone and in the neuropil at region where the CeL will develop (*asterisk*). Scale bar=300 μm. In all cases, *arrow* indicates the region from which the insert (4×) was taken

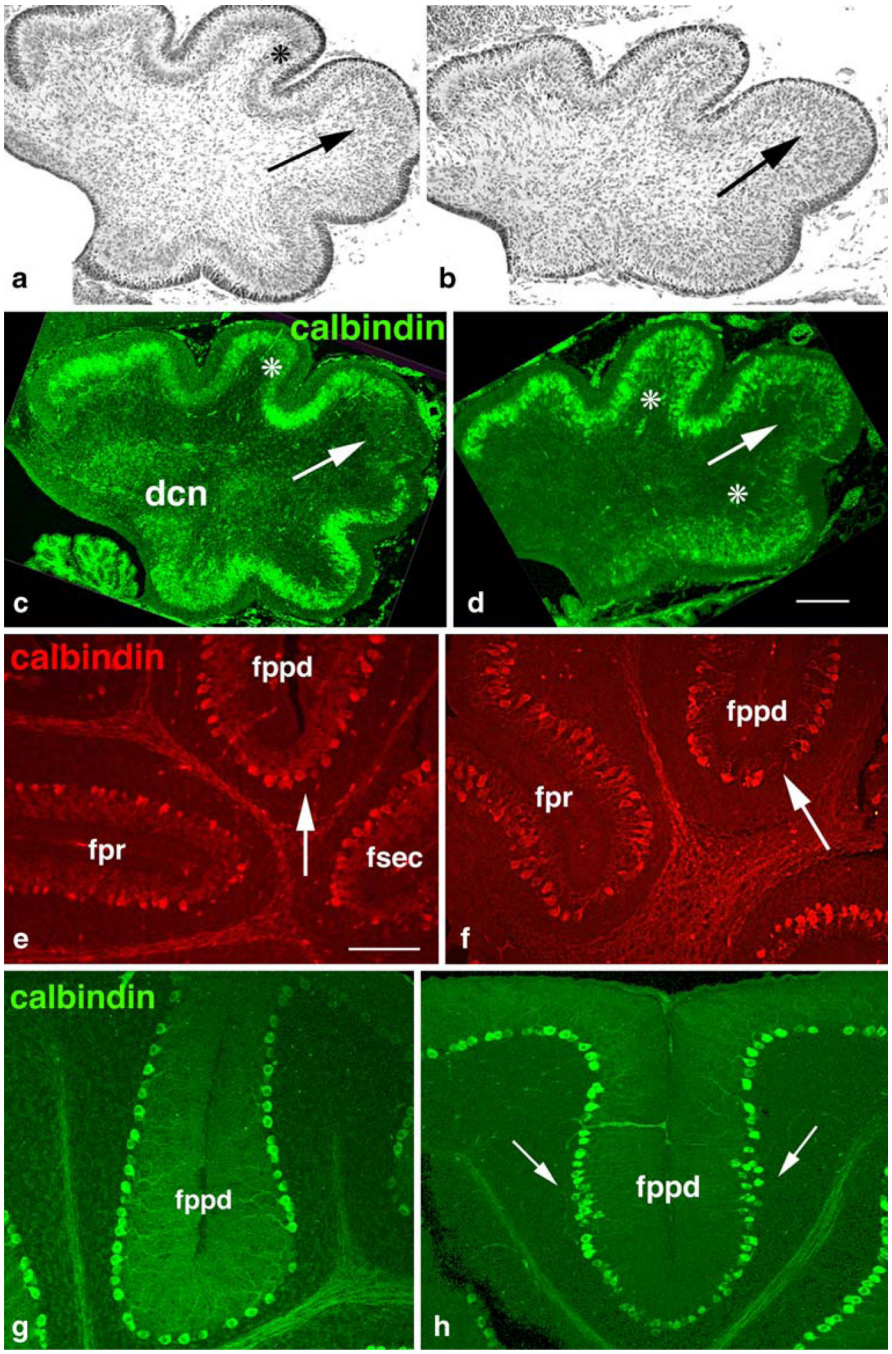

Fig. 5.

Purkinje cell maturation. **a, b** Nissl staining of midsagittal sections at P0 demonstrating coalescence of PCs into a monolayer at P0. GAP-43 (+/+) (**a**) and GAP-43 (−/−) (**b**). **a** Purkinje cells have begun coalescing into a monolayer (*asterisk*) except in the CeL (*arrow*). **b** Increased cell density in the CeL (*arrow*). **c–h** Calbindin expression by PCs. GAP-43 (+/+) (**c, e, g**) and GAP-43 (−/−) (**d, f, h**). **c, d** Midsagittal sections at P0. **c** PCs have begun to coalesce into a monolayer (*asterisk*) but are excluded from the CeL where the fppd is beginning to invaginate (*arrow*). **d** PC migration into the anterior and posterior lobes is

inhibited (*asterisks*) and they invade the CeL (*arrow*). Scale bar=50 μm. **e, f** Expression of calbindin by PCs at P8. **e** PCs flanking primary (*fpr*) and secondary (*fsec*, fppd) fissures are elaborating extensive dendritic arbors (*arrow*). **f** GAP-43 (−/−) PCs flanking the secondary fppd have stunted dendrites (*arrow*) and are misaligned. Scale bar= 150 μm. **g, h** Expression of calbindin by PCs at P21. **g** PCs flanking the fppd form a mono-layer. **h** PCs flanking the fppd remain aggregated at the fissure flanks (*arrows*). Scale bar=100 μm

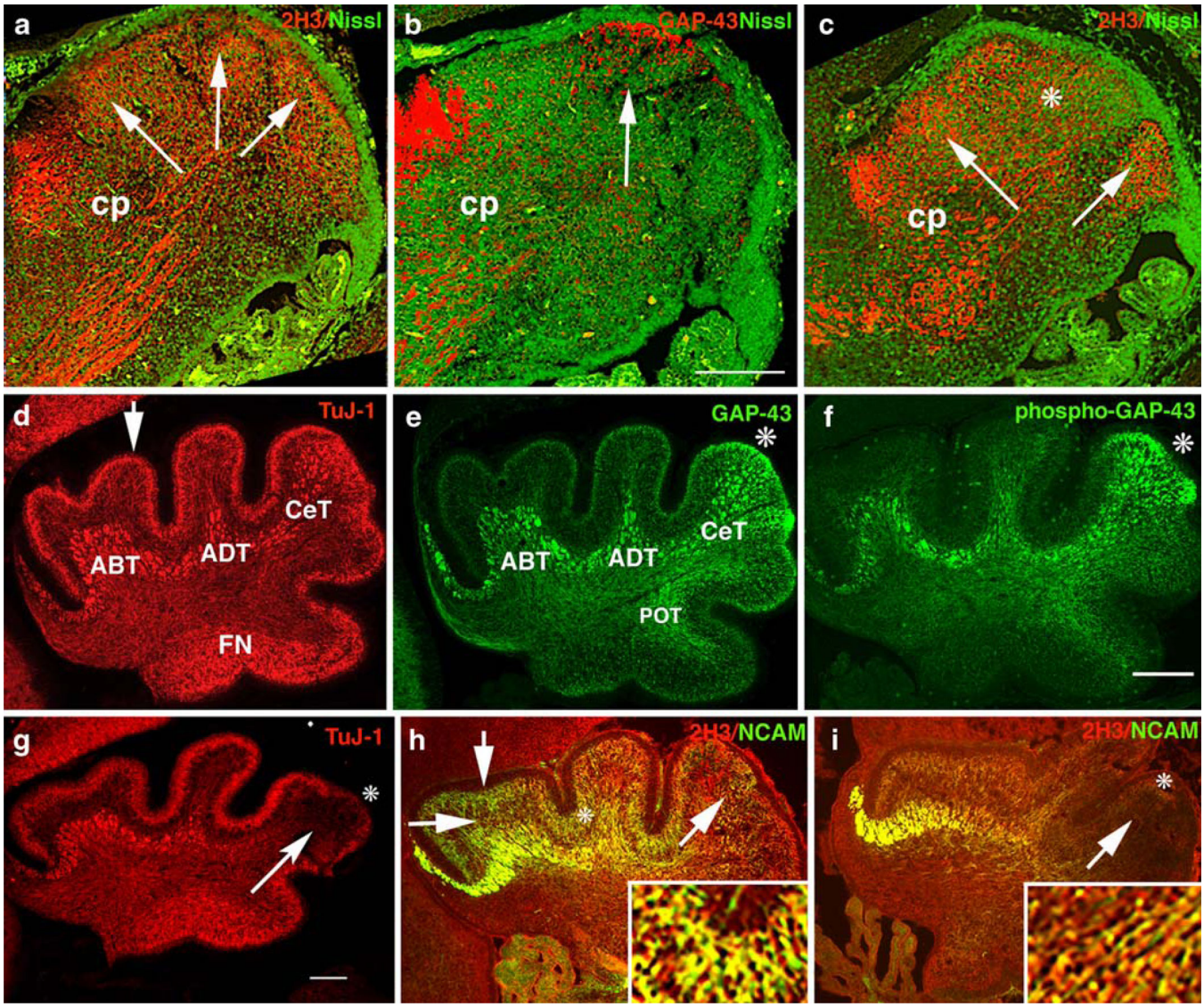

Fig. 6.

Innervation of the developing cerebellum. **a–c** Neurons in the differentiating neuropil of the midsagittal cerebellar anlage at E17.5 detected with 2H3 or GAP-43 (*red*) and Nissl (*green*). GAP-43 (+/+) (**a, b**) and GAP-43 (−/−) (**c**). **a** *Arrow*s indicate the nascent primary lobes containing 2H3 labeled fibers and cerebellar peduncle (*Cp*) inputs and outputs. **b** GAP-43 is concentrated in neurons at the developing CeL subjacent to the EGL (*arrow*) and in Cp fibers. c In the absence of GAP-43, there is an overall decrease in 2H3-labeled fibers especially in the CeL (*asterisk*). **d–g** Neurons in the vermis at P0 detected with TuJ-1, GAP-43, and phospho-GAP-43. GAP-43 (+/+) (**d–f**) and GAP-43 (−/−) (**g**). **d** TuJ-1 labels afferent fiber tracts (*ABT*, ADT, CeT, POT, and IT), the ML (*arrow*), and the fastigial nucleus (*FN*). **e** GAP-43 is enriched in a subset of afferent fiber tracts and the ML of the CeL (*asterisk*). **f** GAP-43 is phosphorylated in afferent fiber tracts that terminate in the CeL. These tracts co-localize in the CeL with ML neurons that also contain highly phosphorylated GAP-43 (*asterisk*). **g** TuJ-1 labeled CeT fibers fail to penetrate the CeL (*arrow*) and label in

the ML is decreased (*asterisk*). **h, i** Lateral sections of the same P0 mice double labeled with 2H3 and NCAM. GAP-43 (+/+) (**h**) and GAP-43 (−/−) (**i**). **h** NCAM-labeled CeT fiber tracts (*diagonal arrow*) and a subset of ML neurons (*asterisk*) in the AL and CeL. The EGL (*vertical arrow*) and PCs (*horizontal arrow*) do not label with either NCAM or 2H3. i In the absence of GAP-43, afferent fibers labeled with NCAM do not penetrate the CeL (*arrowhead*) and ML neurons are not labeled with NCAM (*asterisk*). 2H3 labeling is also reduced in the CeL (*arrow*). Inserts (4×) in **h** and **i** show double labeling of NCAM and GAP-43 (**h**) or 2H3 (**i**). In all cases, scale bar=300 μm

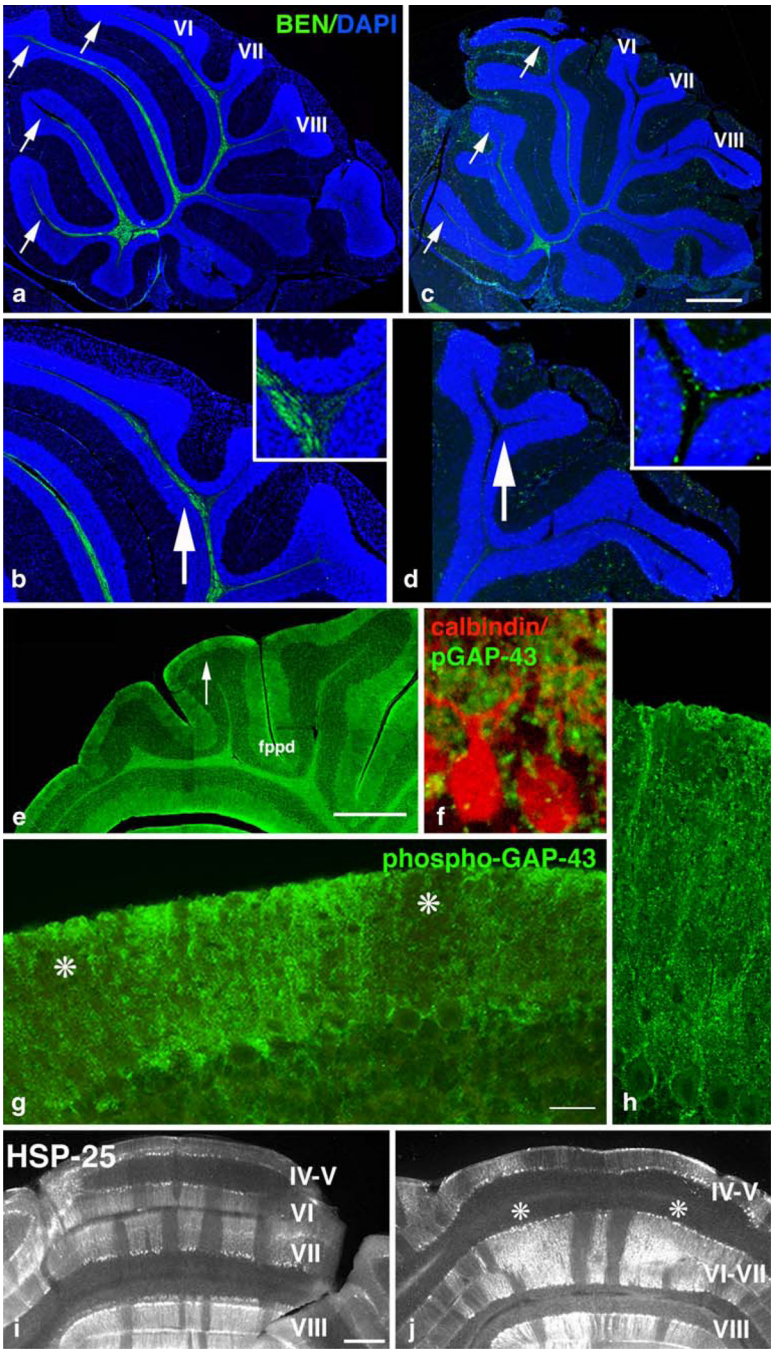

Fig. 7.

Input and output in the mature cerebellum. **a–d** Climbing fiber input to the cerebellar vermis at P21 detected with BEN antibody. Sections counterstained with DAPI. GAP-43 (+/+) (**a, b**) and GAP-43 (−/−) (**c, d**). **a** BEN-labeled CFs penetrate the white matter tracts throughout the anterior and central lobe especially lobules II–VI (*arrows*). **b** Higher power indicating BEN labeled afferents in the fiber bundle penetrating lobule VI. Insert (4×) showing orientation of BEN-labeled fibers at the base of the fps that bisects VI/VII. **c** In the absence of GAP-43, BEN-labeled CFs are abundant only in lobules II– V (*arrows*). d Higher power

indicating BEN-labeled fibers are significantly reduced in the CeL, especially lobule VI/VII (*arrow*). Insert (4×) showing misorientation of BEN-labeled fibers at the base of the fps. Scale bars: **a**=1 mm; **c**= 750 μm; **b** and **d**=300 μm. **e–g** Presynaptic terminals synapsing on PCs at P8 labeled with phosphorylated GAP-43. PCs detected with calbindin. **e** Lower power showing areas enlarged in (**f–h**). **f** Phosphorylated GAP-43 in presynaptic terminals on PC cell bodies and proximal dendrites. **g** Higher power of *arrow* in **e** showing patchy distribution of phosphorylated GAP-43 throughout the ML (*asterisks*). **h** Phosphorylated GAP-43 in presynaptic terminals on distal PC dendrites. Scale bars: **e**= 500 μm, **f**=30 μm, **g**=100 μm, **h**=50 μm. **i, j** Parlobular stripes of PCs in coronal sections at P30 labeled with anti-heat shock protein-25 (*HSP-25*). GAP-43 (+/+) (**i**) and GAP-43 (−/−) (**j**). **i** Characteristic mediolaterally patterned bands, especially in folia VI and VII. **j** In the absence of GAP-43 in this example, the fps separating folia VI/VII is absent. The stripe pattern in folia VI is disrupted (*asterisks*). Scale bar=500 μm

Table 1

Differences between GAP-43 (+/+) and (−/−) mice in area of each cerebellar folia and depth of each fissure

Zone	Folia	Area as % of (+/+)	Fissure	Depth as % of (+/+).
AZ	I–II	57±6.1*	Fprc	64.1±3.7*
	III	79±14.7	Fpc	70±4.7
	IV–V	93±6.4		
CZ	VI–VII	43±9.8*	Fpr	77±3.0*
PZ	VIII	86±5.6	Fppd	74±10.9*
NZ	IX	75±8.7*	Fsec	87±4.0*
	X	66±6.1**	Fpl	68±7.6*

Brains from six littermate pairs of GAP-43 (+/+) and (−/−) P21 mice were fixed in 4% PFA and 14-μm paraffin parasagittal sections at the vermis Nissl-stained. The area occupied by each folia (delineated from the base of the adjacent fissure) and the depth of each fissure was calculated from digital images of sections taken from the vermis using IP lab. Results are expressed as ±SEM. Folia in the anterior, central, and nodular zones were all reduced in size. Likewise, the secondary fissures within each folia were also significantly reduced in depth.

* $p<0.05$,

** $p<0.001$, two sided Mann–Whitney test, $n=6$